INTERNATIONAL JOURNAL FOR NUMERICAL METHODS IN FLUIDS
Int. J. Numer. Meth. Fluids 2005; **49**:1033–1051
Published online 11 August 2005 in Wiley InterScience (www.interscience.wiley.com). DOI: 10.1002/fld.1044

Inviscid flow modelling using asymmetric implicit finite difference schemes

H. C. de Lange*,†

Department of Mechanical Engineering, Technische Universiteit Eindhoven, 5600 MB Eindhoven, The Netherlands

SUMMARY

Asymmetric spatial implicit high-order schemes are introduced and, based on Fourier analysis, the dispersion and damping are calculated depending on the asymmetry parameter. The derived schemes are then applied to a number of inviscid problems. For incompressible convection problems the proposed asymmetric schemes (applied as upwind schemes) lead to stable and accurate results. To extend the applicability of the proposed schemes to compressible problems acoustic upwinding is used. In a two-dimensional compressible flow example acoustic and conventional upwinding are combined. Evaluation of all presented results leads to the conclusion that, of the studied schemes, the implicit fifth order upwinding scheme with an asymmetry parameter of about 0.5 leads to the optimal results. Copyright © 2005 John Wiley & Sons, Ltd.

KEY WORDS: inviscid; asymmetric; spatial implicit; upwinding; subsonic

1. INTRODUCTION

High speed flows are important in gasturbines, airplanes, etc. Through the development in computing facilities direct numerical simulations (DNS) and large eddy simulations (LES) of these flows are now accessible. This results in the need for suitable unsteady flow solvers. Traditionally, these simulations are performed using spectral methods. However, over the last decade compact implicit finite difference methods [1] have been successfully developed. These schemes combine high-order accuracy with spectral-like resolution properties. The originally proposed implicit schemes were symmetric, i.e. central, differences schemes which were employed to the convective as well as for diffusive contributions of the Navier–Stokes equations. This meant that they could only be used when the grid-Reynolds number was small enough. For flows at larger Reynolds numbers the non-linear convection term transfer energy

*Correspondence to: H. C. de Lange, Department of Mechanical Engineering (wh2.126), Technische Universiteit Eindhoven, 5600 MB Eindhoven, The Netherlands.
†E-mail: h.c.d.lange@tue.nl

Received 24 January 2005
Revised 5 April 2005
Accepted 11 April 2005

from lower to higher wavenumbers in absence of (or with minor) diffusion this energy will be stored at the highest wavenumbers. This leads to undamped growth of the Nyquist wave.

In, e.g. Reference [2] asymmetric spatial implicit schemes are proposed to supply high-wavenumber damping, to secure that the solution remains numerically stable on all represented wavenumbers. In the present paper the same technique will be explored. It will be shown that with these asymmetric implicit schemes it is possible to accurately solve flows even at infinite Reynolds numbers. Three different spatial discretization scheme-types are treated: explicit third (E3), implicit third (I3) and implicit fifth (I5) order schemes. Fourier analysis shows that the dispersion and damping of the schemes is determined by the degree of asymmetry of the schemes which is determined by means of an asymmetry parameter.

Two examples of inviscid incompressible flows are presented. As a first step, it is shown that the asymmetric schemes give good results in the Molenkamp-test. This test involves linear transport of a passive-scalar. Next, the analysis is extended to a non-linear convection problem: solving the inviscid Burgers equation. In this problem the solution steepens to a discontinuity. It will be shown that the proposed asymmetric schemes lead to stable and accurate results.

In compressible subsonic flows the non-linear flow behaviour is contained within the propagation of the characteristic acoustic waves. This means that application of the asymmetric schemes only to the convective fluxes is insufficient to damp the high wavenumber modes. For this reason a new approach was proposed in Reference [3]. In this approach the characteristic waves are used as the basic flow phenomenon. The asymmetry is used along the propagation velocity of these waves. This technique will be introduced as 'acoustic upwinding'. It will be shown, by means of a number of examples, that acoustic upwinding leads to accurate results and that (depending on the choice of the asymmetry parameter) it indeed dampens the non-representable waves effectively. First, a one-dimensional example demonstrates that the propagation of acoustic waves is accurately predicted. Next, a convection dominated problem is treated which shows the possibilities of the proposed schemes for mildly compressible flows. In the last example acoustic and conventional upwinding are combined in a two-dimensional problem.

2. SCHEMES

Similar to the introduction of symmetric schemes in Reference [1], we start from an implicit coupling of the function values on a set of nodes (f_i) to a linear combination of the values of the first derivative (f'_i)

$$\alpha_1 f'_{i-1} + f'_i + \alpha_2 f'_{i+1} = b_1 \frac{f_i - f_{i-2}}{2h} + a_1 \frac{f_i - f_{i-1}}{h} + a_2 \frac{f_{i+1} - f_i}{h} + b_2 \frac{f_{i+2} - f_i}{2h} \tag{1}$$

In the analysis presented in Reference [1] the values of the left and right coupling constants are taken symmetrically, i.e. $\alpha_1 = \alpha_2$, $b_2 = b_1$, etc. Similar to Reference [2], we leave an opening for non-equal coefficients. There is of course no limit to the extension to which the stencil could theoretically be stretched. However, to retain the compactness of the stencil we have restricted the analysis to schemes which lead to five-point coupling. This means that we do not consider the coupling with nodes $i + 3$ and $i - 3$. Furthermore, the implicit coupling is restricted to three point (tridiagonal) coupling to reduce the computational effort necessary.

To find the relations between the coefficients, the Taylor-series expansions are coupled at various orders. Matching these equations at the desired error leads to the following constraints:

First order:

$$a_2 + a_1 + b_2 + b_1 = 1 + \alpha_2 + \alpha_1$$

Second order:

$$\tfrac{1}{2}(a_2 - a_1) + b_2 - b_1 = \alpha_2 - \alpha_1$$

Third order:

$$\frac{1}{3!}(a_2 + a_1) + \frac{2^2}{3!}(b_2 + b_1) = \frac{1}{2}(\alpha_2 + \alpha_1)$$

Fourth order:

$$\frac{1}{4!}(a_2 - a_1) + \frac{2^3}{4!}(b_2 - b_1) = \frac{1}{3!}(\alpha_2 - \alpha_1)$$

Fifth order:

$$\frac{1}{5!}(a_2 + a_1) + \frac{2^4}{5!}(b_2 + b_1) = \frac{1}{4!}(\alpha_2 + \alpha_1)$$

Sixth order:

$$\frac{1}{6!}(a_2 - a_1) + \frac{2^5}{6!}(b_2 - b_1) = \frac{1}{5!}(\alpha_2 - \alpha_1)$$

Note that, for any symmetric set of coefficients, the even order equations are automatically satisfied. Therefore, the added degrees of freedom due to the asymmetric schemes also leads to an added set of constraints (and not to a higher order of the truncation error). The restriction to the five point stencil with tri-diagonal implicit coupling leads to the restriction to fifth (for asymmetric schemes) and sixth (for symmetric schemes) order. Therefore, in this paper third and fifth order asymmetric schemes will be compared, similar to Reference [4].

3. SCHEME ANALYSIS

To analyse the schemes we use the spectral analysis proposed in Reference [1]. In this analysis the function values are decomposed into their Fourier components. Next, a scaled wavenumber $z \equiv 2\pi k/N$ and coordinate $s \equiv x/h$ are introduced. The Fourier modes can then be represented by $\exp(\mathrm{i}zs)$ (with $\mathrm{i}^2 = -1$). The exact first derivative becomes a function with coefficients: $\hat{f}'_k = \mathrm{i}z\hat{f}_k$. The differencing error can now be found by solving the modified wavenumber z' for each z from

$$\mathrm{i}z' = \frac{b_1(1 - \mathrm{e}^{-2\mathrm{i}z})/2 + a_1(1 - \mathrm{e}^{-\mathrm{i}z}) + a_2(\mathrm{e}^{\mathrm{i}z} - 1) + b_2(\mathrm{e}^{2\mathrm{i}z} - 1)/2}{1 + \alpha_1\mathrm{e}^{-\mathrm{i}z} + \alpha_2\mathrm{e}^{\mathrm{i}z}}$$

Exact differentiation corresponds to $z' = z$. Differences in the real part (z'_r) of z' imply a dispersion error in the scheme, while the imaginary part (z'_i) of z' indicates its damping. For all different schemes that will be derived the results of this analysis are presented in Figure 1.

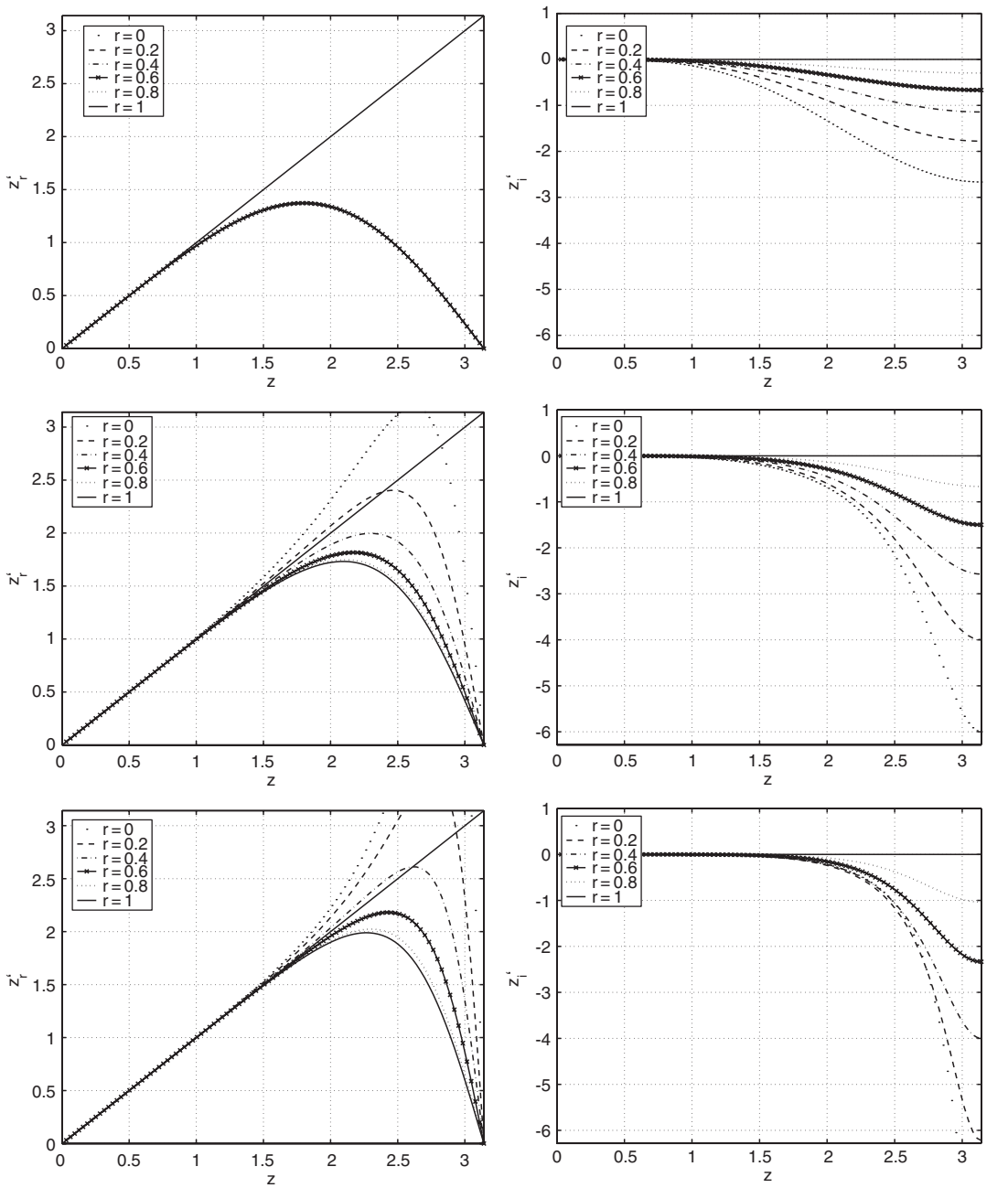

Figure 1. The modified real (left: z'_r) and imaginary (right: z'_i) wavenumber as function of the imposed wavenumber (z) for explicit (top), third-(middle) and fifth-order (bottom) schemes as a function of the asymmetry parameter ratio $r \equiv a_2/a_1$.

A first set of schemes can be found when the α's are taken equal to zero. This means that the coupling in Equation (1) becomes explicit. The truncation order to which the constraints can be met is then limited to four. This means $b_2 = b_1 = -\frac{1}{6}$ and $a_2 = a_1 = \frac{2}{3}$. A truncation error of the third order leads to an additional degree of freedom in which the asymmetry can be a free parameter, e.g. by imposing the asymmetry parameter r

$$r \equiv a_2/a_1$$

The effect of the asymmetry on the third order explicit schemes can be seen in Figure 1 (top). Clearly, the dispersion error (right) due to the misrepresentation of the real part of z does not depend on the wavenumber. However, the asymmetry does induce an imaginary part in the modified wavenumber. The induced damping starts at z-values of about $\pi/6$ (equivalent to $k = N/12$).

To reduce the damping and the dispersion error of the fully explicit schemes, we now use implicit tridiagonal coupling. This means that the α's can be non-zero. Furthermore, the values of b_1 and b_2 are set to zero to retain the order of the scheme. The number of free parameters is four (a_1, a_2, α_1 and α_1). When using symmetric differencing the classical fourth order Pade scheme is retrieved. As before, the introduction of the asymmetry parameter r, reduces the order of the scheme to third order. The resulting modified wavenumbers z'_r (right) and z'_i (left) are shown in Figure 1 (middle). It becomes clear that the dispersion error is smaller for r not equal to one. This shows (similar to the conclusions in Reference [1]) that the truncation error may not be the best basis to judge the schemes spectral behaviour. With respect to the dispersion error, asymmetric schemes with r equal to approximately 0.2–0.3 seem to give the best result. Again, the asymmetry also implies damping. However, as compared to the explicit schemes, this damping now seems to be more restricted to higher wavenumbers. It starts at z-values of about $\pi/3$ (equivalent to $k = N/6$).

A next step is to increase the order of the scheme by re-introducing non-zero b-values. This gives the scheme six free parameters. Obviously, this means that the resulting scheme will now be sixth order with symmetric parameters. On the other hand, if asymmetry is imposed, the resulting schemes will have a fifth order truncation error. In Figure 1 (bottom) we show the spectral behaviour of these schemes. Again, compared to the previous schemes, the results clearly have improved. The dispersion error shows that the fifth order schemes perform better than the sixth order scheme. The optimum (minimum dispersion error) appears at r-values of about 0.4–0.5. In this case the deviation of z'_r from z starts at z-values of approximately $2\pi/3$. This goes more or less hand in hand the introduced damping error, which starts at z-values of approximately $\pi/2$ (equivalent to $k = N/4$). Comparison with the CULD and CUHD schemes proposed in Reference [5] and used in Reference [3] shows that the spectral behaviour of those (penta-diagonal) schemes is similar to that of the fifth order implicit scheme with $r = 0.5$.

From here on, the different scheme-type will be indicated by a name in which the letter indicates the type of scheme (E: explicit and I: implicit), the number indicates the order of the truncation error. The parameters (which depend on r) for each of these schemes are given in the Appendix. At this point it is useful to note that for r equal to $\frac{1}{3}$ the I3-scheme excludes influence of f_{i+1} since a_2 then equals zero. Similarly, for r equal to $\frac{5}{9}$ the I5-scheme becomes independent of f_{i+2} (b_2 then equals zero).

4. INCOMPRESSIBLE FLOW

To show the effect of the proposed schemes they are tested in two model test problems: the Molenkamp test and the formation of a shock in the inviscid Burgers equation. In these tests the asymmetry is used as an upwinding scheme. In other words $r = r_c$ for positive velocities and $r = 1/r_c$ for negative velocities. For the time discretization we use a third order Runge–Kutta scheme [6].

4.1. Molenkamp test

For a first evaluation of the asymmetric implicit upwinding schemes, the two-dimensional Molenkamp test is used. This is done by transporting a passive tracer in a prescribed fixed-disc velocity field. The deformation of the initial tracer distribution measures the error of the scheme. The equation to be solved is

$$\frac{\partial f}{\partial t} = -u(x, y)\frac{\partial f}{\partial x} - v(x, y)\frac{\partial f}{\partial y}$$

with

$$u(x, y) = 2\pi y$$

$$v(x, y) = -2\pi x$$

on the domain

$$-1 < x \leqslant 1, \quad -1 < y \leqslant 1$$

The initial distribution (at $t = 0$) is

$$f(x, y) = 0.01^{-\alpha r^2}, \quad r = \sqrt{(x + \tfrac{1}{2})^2 + y^2}$$

with $\alpha = 32$. Note that α is chosen larger than f.e. in Reference [7]. This is done to obtain a high activity innerfield, while the boundaries are and remain close to zero. Therefore, the treatment of the boundary has no influence.

For all schemes the boundary discretization is performed using a one-sided implicit scheme

$$f_1' + 2f_2' = \frac{1}{h}\left(2f_2 - 2\frac{1}{2}f_1 + \frac{1}{2}f_3\right)$$

for the boundary point and the fourth order Pade scheme (I3($r = 1$)) for the second point.

At $t = 1$ the profile has undergone one complete revolution. The exact solution at this time (f_{ex}) equals the initial solution. In Figure 2 the rms of the error ($||\Delta f||_2$) as a function of the asymmetry parameter r is presented for the three different scheme types. A first clear conclusion is that all (nearly) symmetric schemes ($r > 0.8$) are unable to solve this problem. The absence of damping of high wavenumber modes leads to unstable solutions. As might be expected, the accuracy of the I5 schemes is superior to that of the other two schemes. This is already true at a fairly low resolution. Obviously, the error for higher resolutions decreases

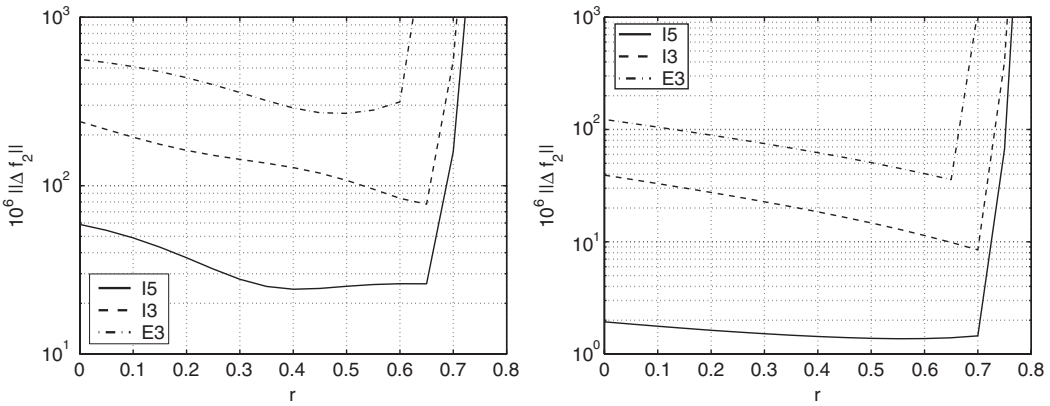

Figure 2. $10^6 \Delta f_2$ (vert. axis) of the Molenkamp test as function of r (hor. axis) for the three different scheme types on a 33×33 (left) and a 65×65 (right) grid.

more rapidly for the I5-scheme. Note that the 33×33-solution with the I5-scheme is already more accurate than the 65×65-solution of the E3-scheme. Comparing the different schemes for varying r shows that the asymmetric schemes give comparable results for all asymmetry parameters. However, the best results are obtained with r approximately 0.4–0.6.

4.2. Burgers equation

In this section we study the effect of the asymmetry parameter on the results of a one-dimensional non-linear convection problem. In this case we solve $u(x,t)$ from

$$\frac{\partial u}{\partial t} = -u\frac{\partial u}{\partial x}$$

which is the Burgers equation for $Re = \infty$. Starting from an initial solution

$$u(x,0) = \sin(\pi x)$$

the solution to this problem is periodic. It is solved the domain

$$-1 < x \leqslant 1$$

At $t = \frac{1}{2}$ the exact solution on the chosen domain is given by

$$x(u,t) = u/2 + \frac{a\sin(u)}{\pi}$$

as shown in Figure 3. Clearly, any scheme with spectral damping will lead to fluctuations close to the $x = \pm 1$. At this time more and more energy is transferred to non-represented wavenumbers, that is, the discontinuity steepens more and more beyond the grid resolution. However, if the scheme is sufficiently asymmetric, stability of the solution is still maintained. Moreover, if the asymmetry parameter is chosen appropriately the spectrum will remain comparable to that of the exact solution. To compare the different schemes we will use the rms

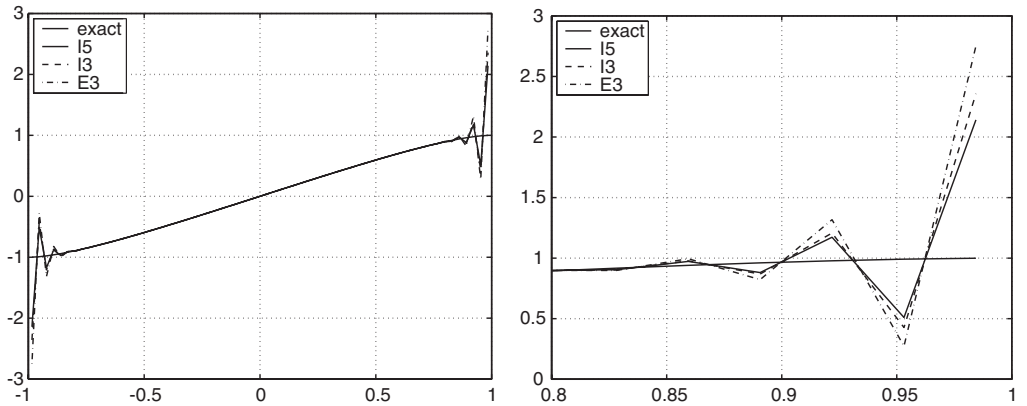

Figure 3. The exact sawtooth Burgers solution (u: vertical axis as function of x hor. axis) at t equal to $\frac{1}{2}$ compared to the numerical solutions using r equal to 0.4 (for $N_x = 64$ and $N_t = 1024$).

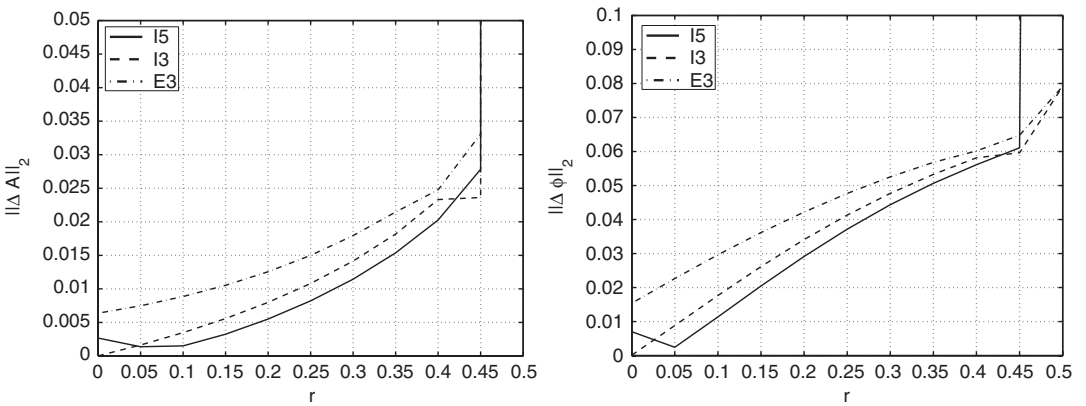

Figure 4. The rms of the energy ($||\Delta A||_2$: left) and phase ($||\Delta\phi||_2$: right) difference of the exact and numerical solution to the Burgers problem for the three different scheme types as function of r (horizontal axis).

of the spectral amplitude and the phase difference

$$||\Delta A||_2 \equiv \sqrt{\frac{\sum_{N/2}(A - A_{\text{ex}})^2}{N/2}}$$

$$||\Delta \phi||_2 \equiv \sqrt{\frac{\sum_{N/2}(\phi - \phi_{\text{ex}})^2}{N/2}}$$

where the sum is take over all available wavenumbers.

This is shown in Figure 4 for three different numerical schemes. Here we used N equal to 128 and 1024 timesteps. Surprisingly, Figure 4 shows that the best solution to this particular problem is found from the I3($r = 0$)-scheme. The reason for this could be that this particular

scheme does not use any downwind information, while it is still third order. For the remainder it is clear that the I5-schemes produce more or less accurate results for all r-values smaller than 0.45. At higher r-values the schemes become unstable. A striking feature of the presented results is that this seems to be true for all considered scheme-types; as soon as r is chosen larger than 0, the results strongly deteriorate. For the sake of completeness it is worthwhile to note that none of the symmetric $(r=1)$-schemes is able to find a solution to this problem.

5. COMPRESSIBLE ONE-DIMENSIONAL FLOW

To include compressiblity into the equations the tests are extended to solve $\rho(x,t)$ and $u(x,t)$ simultaneously

$$\frac{\partial \rho}{\partial t} = -\frac{\partial \rho u}{\partial x}$$

$$\frac{\partial u}{\partial t} = -u\frac{\partial u}{\partial x} - \frac{1}{\rho}\frac{\partial p}{\partial x}$$

to complete this set of equations the pressure p needs to be connected to the density ρ. In the examples presented here, the entropy will be assumed constant. Therefore, the isentropic compression relation may be used

$$\frac{p}{p_\infty} = \left[\frac{\rho}{\rho_\infty}\right]^\gamma$$

where p_∞ and ρ_∞ indicate the pressure and density in the reference state. For this atmospheric conditions are chosen: $\rho_\infty = 1.2\,\mathrm{kg/m^3}$ and $T_\infty = 300\,\mathrm{K}$. Furthermore, the following properties to describe the medium (air) are used: $R_g = 287\,\mathrm{J/kg\,K}$ and $\gamma = 1.4$.

5.1. Acoustic upwinding

The behaviour of the proposed schemes in compressible flows is explored in the following problem. At t is zero the pressure $p(x,0)$ and velocity $u(x,0)$ are prescribed on the periodic domain $0 < x \leqslant 1$ by

$$u(x,0) = 0$$

$$p(x,0) = p_\infty + \delta p \frac{\tanh(D\sin(2\pi x))}{\tanh(D)}$$

with δp the amplitude of the wave and the parameter D gives the wave steepness. As long as the amplitude of the wave is small (such that the speed of sound c can be chosen approximately constant) the exact solution of this problem will be repetitive. In between the pressure profile will change shape, however, note that the points at which $p = p_\infty$ will not move. Therefore, these initial conditions lead to a stationary wave. Since there is no physical damping nor dispersion (if $c = c_\infty$), the initial solution will be restored after a time $t = k_t/c_\infty$ for any positive integer k. This should be true for both the velocity as well as for

the pressure. In this analysis we will use the solution for $k_t = 1$ and use 1024 timesteps and 64 gridpoints. The wave parameters are chosen: $D = 20$ and $\delta p = 10^{-4} p_\infty$.

A first approach to this problem is the use the asymmetric schemes only as an upwinding scheme for the non-linear convective term. In Figure 5 (left) an example of the result of these simulations is shown. In this example the fifth order implicit scheme is used for the convective term, while the other terms are all discretized using the central sixth order (I5($r = 1$))-scheme. Clearly, these simulations lead to highly oscillative solutions. The damping provided by the asymmetric convective term is not sufficient to prevent these non-physical oscillations to appear. This means that, if the numerical damping must take care of the occurrence of non-physical (high-wavenumber) compression waves, the asymmetric schemes should be applied in a different way.

In this paper we use an approach as proposed in Reference [3]. It starts from reformulating the compressible flow equations. For this the Local One-Dimensional Inviscid (LODI)-relations [8] are used, which are based on the characteristic wave formulation

$$\begin{aligned} \frac{\partial \rho}{\partial t} &= \frac{-1}{2c^2}(\mathscr{L}_{1x} + \mathscr{L}_{5x}) \\ \frac{\partial u}{\partial t} &= \frac{1}{2\rho c}(\mathscr{L}_{1x} - \mathscr{L}_{5x}) \end{aligned} \tag{2}$$

where $\mathscr{L}_{1x}$ and $\mathscr{L}_{5x}$ are defined as

$$\mathscr{L}_{1x} = (u - c)\left(\frac{\partial p}{\partial x} - \rho c \frac{\partial u}{\partial x}\right)$$

$$\mathscr{L}_{5x} = (u + c)\left(\frac{\partial p}{\partial x} + \rho c \frac{\partial u}{\partial x}\right)$$

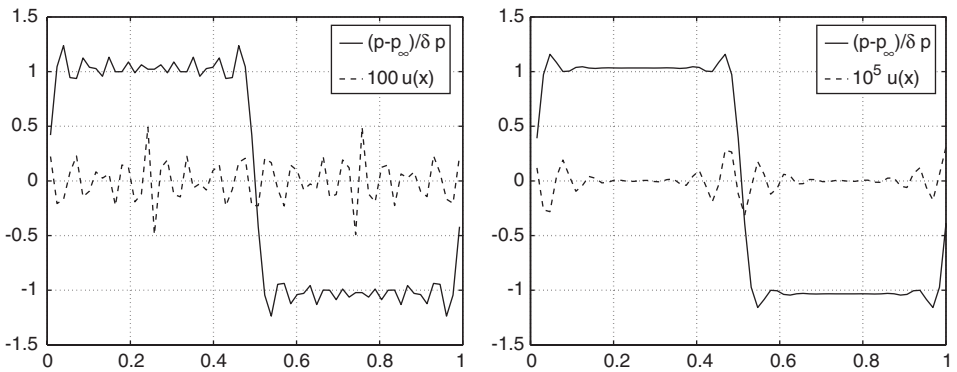

Figure 5. The pressure ($(p - p_\infty)/\delta p$) and velocity (u) as function of x (horizontal axis) for $k_t = 1$ with upwinding (I5($r = 0.5$)) applied only to the convective term (left) and with acoustic upwinding (right). Specially note that: left $u \times 10^2$ and right $u \times 10^5$.

Note that $\mathscr{L}_{1x}$ and $\mathscr{L}_{5x}$ represent the characteristic waves travelling with the velocities $u-c$ and $u+c$, respectively. Now, we apply a technique which we will call acoustic upwinding, i.e. the differentials in both wave descriptions are discretized using the wave velocity as the upwind direction.

To see the effect of this acoustic upwinding we first look at the result in Figure 5 (right). In this figure again the I5($r=0.5$)-scheme is used, but now applied for acoustic upwinding. Now it is obvious that the use of the asymmetric schemes in this way leads to the damping of the numerical oscillations. This leads to a decrease in the velocity fluctuations of a factor 1000. Furthermore, the structure of the pressure wave remains intact. Indicating that the damping is restricted to the high-wavenumbers. To show this in more quantitatively the rms of both variables

$$||\Delta u||_2 \equiv \frac{\rho_\infty c_\infty}{\delta p}\sqrt{\frac{\sum_N (u(x,1/c_\infty)-u(x,0))^2}{N}}$$

$$||\Delta p||_2 \equiv \frac{1}{\delta p}\sqrt{\frac{\sum_N (p(x,1/c_\infty)-p(x,0))^2}{N}}$$

is presented in Figure 6. The results for $||\Delta p||_2$ show that the rate to which the shape of the initial pressure distribution is recaptured does depend on the type of scheme. The I5-schemes are all more accurate than the other two. However, when comparing the I5-schemes at different r-values it appears that their accuracy is more or less comparable. Only at values of r above 0.9 the oscillations become large enough to show in the rms. For all other values of r the main contribution to $||\Delta p||_2$ is situated at the gridpoints just left and right of $x=0.5$. For the asymmetric schemes this is the area where probably the damping has its most important effect. As the scheme becomes more symmetric (has less damping) the dispersive error takes over and starts to generate high wavenumber oscillations. From the presented $||\Delta u||_2$ it becomes clear that for the implicit I3 and I5-schemes the oscillations can be effectively damped.

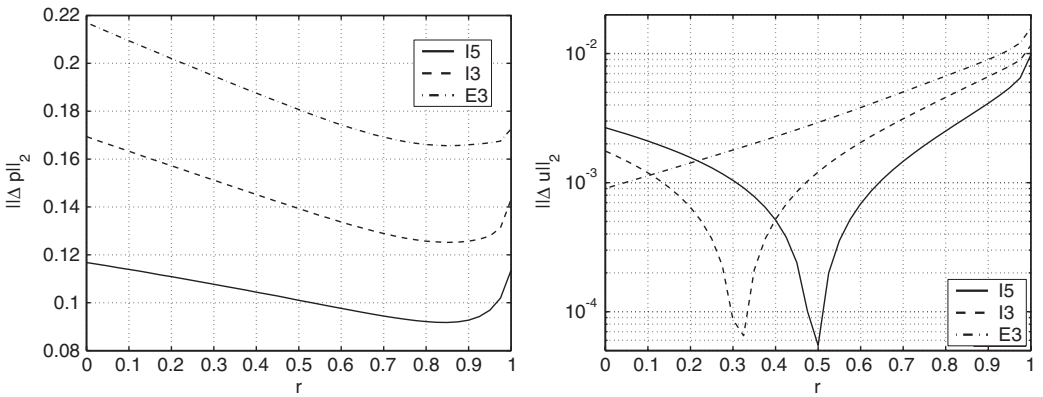

Figure 6. The rms of pressure ($||\Delta p||_2$) and velocity ($||\Delta u||_2$) for $k_t=1$ using acoustic upwinding and I5, I3 and E3-schemes as function of r (horizontal axis).

Furthermore, it appears that at specific r values the dispersive and damping errors more or less cancel, for the I3 scheme this is true at $r \approx \frac{1}{3}$ for the I5-scheme this point lies at $r \approx \frac{1}{2}$.

5.2. Acoustic wave propagation

The proposed acoustic upwinding makes use of the flow equations based on the characteristic waves. It could, therefore, be very useful to determine the effect of the schemes on travelling acoustic waves. These are found if the following initial solution is imposed:

$$p(x,0) = p_\infty + \delta p \frac{\tanh(D\sin(2\pi x))}{\tanh(D)}$$

$$u(x,0) = \frac{\delta p}{\rho c} \frac{\tanh(D\sin(2\pi x))}{\tanh(D)}$$

In the exact solution this will give $\mathscr{L}_{1x} = 0$, and therefore, lead to an exact solution which only includes $\mathscr{L}_{5x}$. Thus, at these initial conditions a wave travelling in the positive x-direction at a speed of c should be found. Note that, in order to be able to predict the exact solution δp should again be chosen small enough. The wave- (D, δp) and medium-parameters (γ, ρ_∞,...) are chosen equal to those in the previous paragraph. Again, the result of the 64-point grid after $t = 1/c_\infty$ in 1024 timesteps will be evaluated.

First, the results of the three schemes are shown in terms of $||\Delta p||_2$ and $||\Delta u||_2$ in Figure 7. In these figures the shape of the rms of p from the previous paragraph can clearly be recognized. However, in this case (as may be expected) $||\Delta u||_2$ and $||\Delta p||_2$ behave similarly. When comparing the results of the three schemes at different values of r, it shows that they perform similarly as long as r is chosen smaller than 0.9 with a minimum error at r approximately 0.8. In Figure 8 the details of the solutions for different r values of the I5-scheme are shown. From this, it is clear that at large r values the spurious waves become dominant. For smaller r values, the differences in the errors are merely due to small changes in

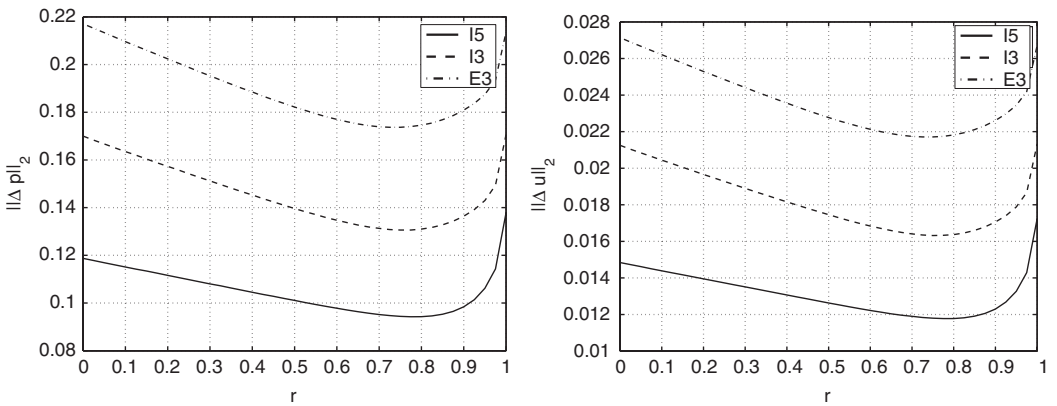

Figure 7. The rms of pressure ($||\Delta p||_2$) and velocity ($||\Delta u||_2$) of the $\mathscr{L}_{5x}$-wave for $k_t = 1$ using acoustic upwinding and I5, I3 and E3-schemes as a function of r (horizontal axis).

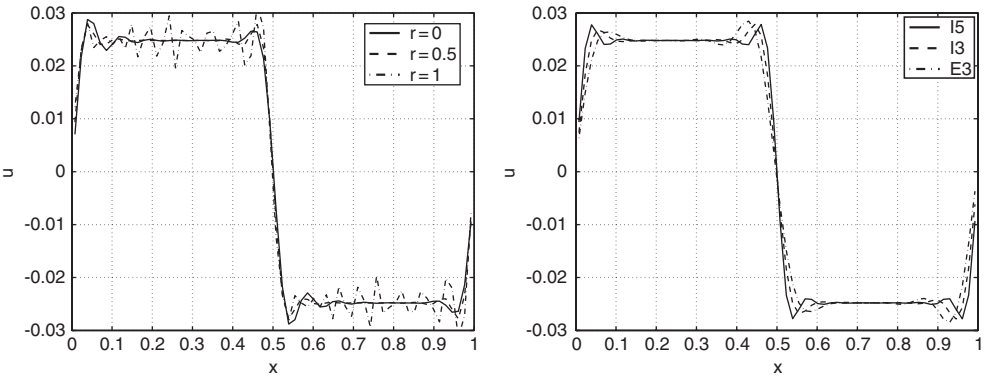

Figure 8. The velocity (u) as function of x (horizontal axis) of the $\mathscr{L}_{5x}$-wave for $k_t = 1$ using acoustic upwinding for the I5-scheme at $r = 0$, 0.5 and 1 (left) and for the I5, I3 and E3-schemes at $r = 0.5$ (right).

the overshoot and its damping close to $x = 0.5$. On the other hand, Figure 7 shows that the error does depend on the type of scheme used. For the E3-scheme the rms values are about a factor 2 larger than the values obtained with the I5-scheme. Details of $u(x, 1/c_\infty)$ (Figure 8 (right)) show that this may be due to the additional damping of the E3- and I3-schemes as compared to the I5-scheme. This causes the decrease of the slope and the longer range to which the damping influences the solution around $x = 0.5$. This behaviour can probably be traced back to the results of the Fourier-analysis. As Figure 1 already showed, the expected extent of the damping decreases by a factor of about 3 between the E3- and I5-schemes.

5.3. *Convection dominated flow*

The examples treated in the previous paragraphs were acoustically (that is pressure wave) dominated. To show the wider applicability of acoustic upwinding to compressible flows a convection dominated problem will now be treated. For this we will now solve a one-dimensional compressible flow equivalent of the inviscid Burgers equation problem as previously described. The governing equations still are the one-dimensional compressible flow equations (2). These will be solved on the domain $0 < x \leqslant 1$ with the initial condition

$$u(x, 0) = Mac_\infty \sin(\pi x)$$

$$p(x, 0) = p_\infty$$

where Ma is the flow Mach number (u_{ref}/c_∞). For a $\gamma = 1$ medium the solution to this problem at t equal to $1/(Mac_\infty)$ is found to be exactly equal to the incompressible Burgers problem (as can bee seen in Figure 9). In that figure the results are presented for $Ma = 0.01$ and $Ma = 0.1$, both solutions are obtained using $N_x = 128$ and $N_t = 8192$. Clearly, the solution at the lower Mach number suffers less from higher wavenumber wiggles. This can be seen more clearly in the zoomed views, where it is obvious that the $Ma = 0.01$-solution still shows a smooth behaviour while the $Ma = 0.1$-solution shows very sharp peaks near to $x = 1$. For flows of different media (different γ) we found that the slope of the profile changes proportional to

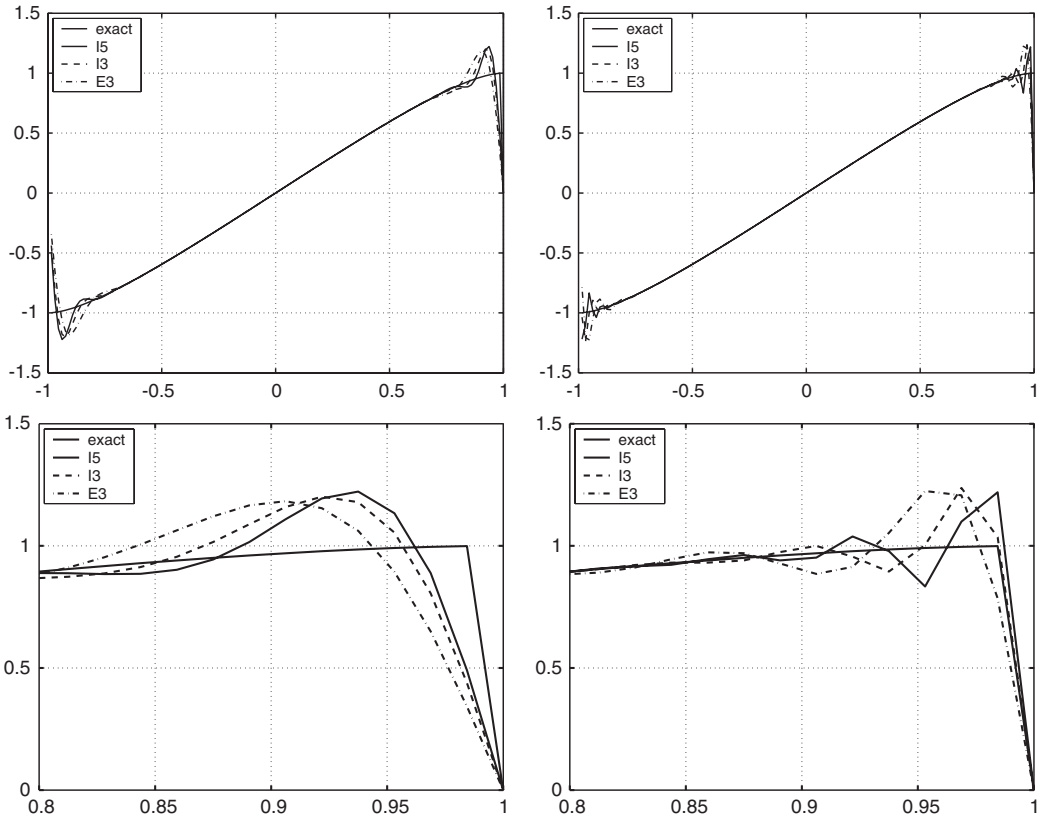

Figure 9. The Burgers solution (u as function of x (horizontal axis) on the full domain (top) and a zoom view (bottom)) at t equal to 0.5 compared to the compressible flow numerical solutions at $1/(Mac_\infty)$ for Ma equal to 0.01 (left) and 0.1 (right) using r equal to 0.6 (for $N_x = 128$ and $N_t = 8192$).

$\gamma^{1/4}$. This is probably due to the interaction of the convective and compressible phenomenae, however, we have not explored this phenomenon in more detail.

Again, Fourier-analysis is used to compare the results obtained with the different schemes. In this case the rmw of the energy $||\Delta A||_2$ and phase $||\Delta\phi||_2$ difference are calculated comparing the exact and numerical solution at t equal to $1/(Mac_\infty)$ normalized as

$$u^*_{1d} \equiv \frac{u}{Mac_\infty}$$

Figure 10 clearly shows that the accuracy of any of the schemes depends on the Mach number. For example, the low r-I5 schemes are unstable for $Ma = 0.01$, while for $Ma = 0.1$ they give accurate results. On the other hand, the E3-schemes show the opposite trend: high accuracy

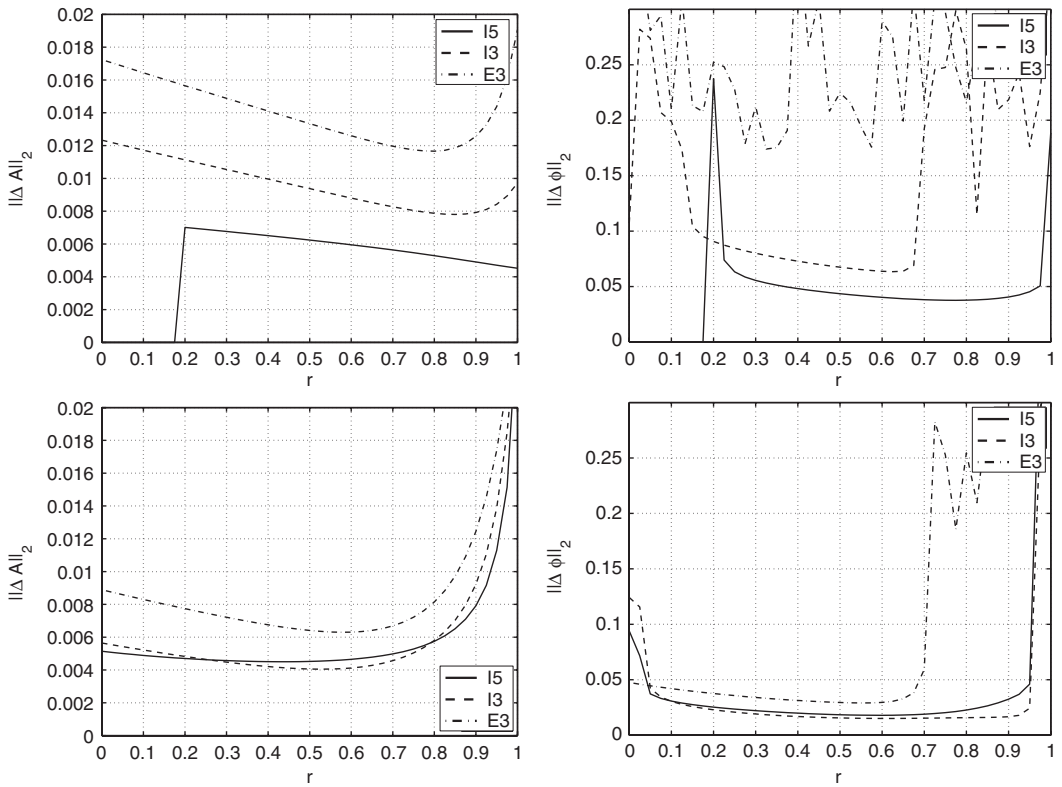

Figure 10. The rms of the energy ($||\Delta A||_2$: left) and phase ($||\Delta\phi||_2$: right) difference of the exact and numerical solution of u_{1d}^* for the one-dimensional compressible Burgers problem for Ma equal to 0.01 (top) and 0.1 (bottom) for the three different scheme types as function of r (horizontal axis).

for $Ma = 0.01$ and instability for $Ma = 0.1$. On the average it appears that in both simulations the I5($0.3 \leqslant r \leqslant 0.5$)- and I3($0.2 \leqslant r \leqslant 0.4$)-schemes give the best performance.

6. TWO-DIMENSIONAL COMPRESSIBLE FLOW

To evaluate the performance of the proposed numerical scheme in more-dimensional flows, the one-dimensional strategy (Equation (2)) is extended to two dimensions. The equations to be solved now are

$$\frac{\partial \rho}{\partial t} = -\frac{\partial \rho u}{\partial x} - \frac{\partial \rho u}{\partial x}$$

$$\frac{\partial u}{\partial t} = -u\frac{\partial u}{\partial x} - v\frac{\partial u}{\partial y} - \frac{1}{\rho}\frac{\partial p}{\partial x}$$

$$\frac{\partial v}{\partial t} = -u\frac{\partial v}{\partial x} - v\frac{\partial v}{\partial y} - \frac{1}{\rho}\frac{\partial p}{\partial y}$$

Again, we propose to use the characteristic wave formulation of this problem

$$\begin{aligned}\frac{\partial \rho}{\partial t} &= \frac{-1}{2c^2}(\mathscr{L}_{1x} + \mathscr{L}_{5x}) + \frac{-1}{2c^2}(\mathscr{L}_{1y} + \mathscr{L}_{5y}) \\ \frac{\partial u}{\partial t} &= \frac{1}{2\rho c}(\mathscr{L}_{1x} - \mathscr{L}_{5x}) - v\frac{\partial u}{\partial y} \\ \frac{\partial v}{\partial t} &= \frac{1}{2\rho c}(\mathscr{L}_{1y} - \mathscr{L}_{5y}) - u\frac{\partial v}{\partial x}\end{aligned} \tag{3}$$

where $\mathscr{L}_{1y}$ and $\mathscr{L}_{5y}$ are defined as

$$\mathscr{L}_{1y} = (v - c)\left(\frac{\partial p}{\partial y} - \rho c\frac{\partial v}{\partial y}\right)$$

$$\mathscr{L}_{5y} = (v + c)\left(\frac{\partial p}{\partial y} + \rho c\frac{\partial v}{\partial y}\right)$$

Note that in this case the cross-wind convection terms have to be separately discretized, which will be done using convective upwinding.

6.1. Acoustic wave

The initial conditions to the two-dimensional wave on the domain $0 < x \leqslant 1$, $0 < y \leqslant 1$ are

$$u(x, y, 0) = 0$$

$$v(x, y, 0) = 0$$

$$p(x, y, 0) = p_\infty + \delta p\frac{\tanh(D\sin(2\pi(x + y)))}{\tanh(D)}$$

To keep the results of the two-dimensional comparable to the previous results, the parameters of the wave and the numerics will be kept the same ($D = 20$, $\delta p = 10^{-4}$, $N_x = N_y = 64$, $k_t = \sqrt{2}$, $N_t = 1024$).

The results of these simulations are analysed using the rms of pressure and velocity vector length according to

$$||\Delta u||_2 \equiv \frac{\rho_\infty c_\infty}{\delta p}\sqrt{\frac{\sum_N (u(x, y, \sqrt{2}/c_\infty) + v(x, y, \sqrt{2}/c_\infty))^2}{N}}$$

$$||\Delta p||_2 \equiv \frac{1}{\delta p}\sqrt{\frac{\sum_N (p(x, y, \sqrt{2}/c_\infty) - p(x, y, 0))^2}{N}}$$

with N the total number of gridpoints ($N_x \times N_y$).

In Figure 11 both properties are presented for the three schemetypes as a function of r. The first striking feature is the resemblance of these figures with the ones found for the one-dimensional calculations (Figure 6). Clearly, the extension of the problem to two dimensions

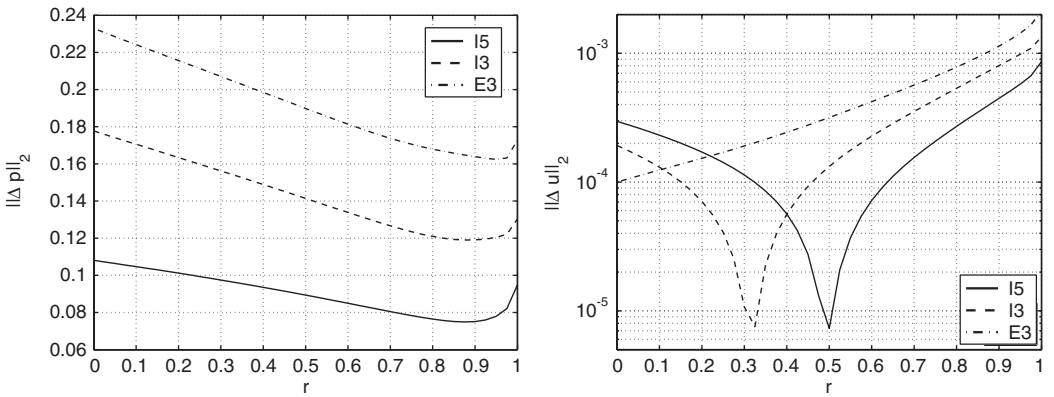

Figure 11. The rms of pressure ($||\Delta p||_2$: left) and velocity ($||\Delta u||_2$: right) of the 2d-acoustic wave for $k_t = \sqrt{2}$ using acoustic upwinding and I5, I3 and E3-schemes as a function of r (horizontal axis).

does not deteriorate the quality of the proposed disretization technique. The solutions found for the I5($r = \frac{1}{2}$) and I3($r = \frac{1}{3}$)-schemes in terms of $||\Delta u||_2$ are again superior to the other solutions. In terms of $||\Delta p||_2$ all I5-schemes produce the best results.

6.2. *Convection dominated flow*

As a last step, the one-dimensional convective analysis will be extended to two-dimensional flow. The inviscid compressible equations (3) will be solved on the domain $0 < x \leqslant 1$ and $0 < y \leqslant 1$ with the initial condition

$$u(x, y, 0) = Mac_\infty \sin(\pi(x + y)) \cos(\theta)$$
$$v(x, y, 0) = Mac_\infty \sin(\pi(x + y)) \sin(\theta)$$
$$p(x, y, 0) = p_\infty$$

Note that these initial conditions should lead to the same solution (at an angle θ with the x-axis) as the one-dimensional convective problem. We will evaluate the results of $\theta = \pi/4$. In this case the solution at $t = \tau$ ($\equiv 1/(\sqrt{(}0.5)Mac_\infty)$) $u(x, 0, \tau)$ should be the same as the one found in the one-dimensional problem. Furthermore, due to symmetry arguments, the same solution should hold for $v(x, 0, \tau)$, $u(0, y, \tau)$ and $v(0, y, \tau)$. Here, as before, the results for $u(x, 0, \tau)$ will be evaluated in terms of $||\Delta A||_2$ and $||\Delta \phi||_2$. In this case u will be normalized as

$$u^*_{2d} \equiv \frac{u}{Mac_\infty \sqrt{2}}$$

Figure 12 shows the results of the simulations for $Ma = 0.1$ using $N_x = 128$ and $N_t = 8192$. For both the amplitude and phase error the implicit schemes clearly show much better results than the explicit schemes. For the E3-results the phase error beyond $r = 0.5$ explodes, the amplitude remains intact. It is striking that the amplitude error of the three scheme types give similar results. Note that these two-dimensional results show a similar behaviour as the

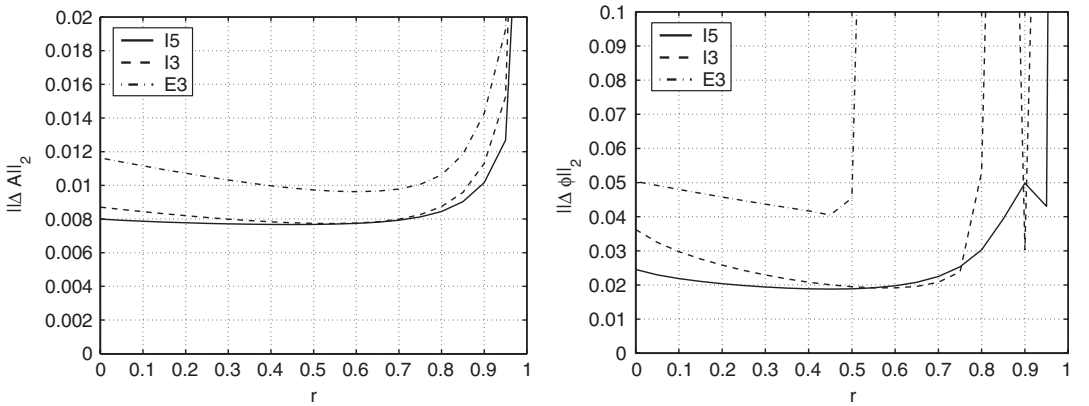

Figure 12. The rms of the energy ($||\Delta A||_2$: left) and phase difference ($||\Delta\phi||_2$: right) of the exact and numerical solution for the two-dimensional compressible Burgers problem for *Ma* equal 0.1 for the three different scheme types as a function of r (horizontal axis).

one-dimensional results in Figure 9. Comparing the different results shows that the best choice would be either a I3- or a I5-scheme with r-values between 0.5 and 0.7.

7. CONCLUSIONS

Asymmetric spatial implicit high-order schemes have been derived similar to Reference [2]. Based on Fourier analysis it has been shown that these schemes are able to accurately represent the spectral properties of the derivatives. The dispersion and damping are calculated depending on the asymmetry parameter r. Clearly, the optimal choice of the scheme depends on the aspired results. The dispersion results show that the fifth order implicit scheme (I5) produces its optimal dispersion result at r-values between 0.4 and 0.5.

Next, the derived schemes have been applied to two model problems: the Molenkamp-test and the formation of a discontinuity ('shock') in the Burgers problem. In both cases the symmetric schemes are not able to solve the problem. For the Molenkamp test r has to be chosen smaller than 0.6–0.7 (depending a little on the scheme-type), while for the formation of the discontinuity from non-linear convection r for all schemes needs to be smaller than 0.45.

When extended to compressible problems, conventional upwinding of the convective contribution to the momentum equations proofs to be insufficient to damp the spurious waves. For this case a new technique: acoustic upwinding is proposed. Thus applied, the I5($r = 0.5$) scheme produces the best results by far in terms of the damping of spurious numerical oscillations. Two-dimensional tests show the same tendency. In this case acoustic and conventional upwinding are combined. For this case the I3 and I5 schemes show comparable results with a slight advantage for the I5 schemes at r-values of about 0.5.

In view of the obtained results the I5-scheme with an asymmetry parameter r of about 0.5 seems to be a promising candidate. It combines the good spectral properties in the Fourier analyses with a numerical damping sufficient to remove spurious waves that result from the energy transfer to non-representable wavenumbers. In this way a highly accurate result without

numerical oscillations can be achieved. These properties lead to satisfactory results in all presented examples. The next step will be to combine this scheme with the splitted time stepping technique (proposed in Reference [9]) in the application to practical flow problems.

APPENDIX A: SCHEME PARAMETERS

The parameters for E3 are

$$\begin{aligned} a_1 &= \frac{4}{3}\frac{1}{1+r} & a_2 &= ra_1 \\ b_1 &= -\tfrac{1}{6} + \tfrac{1}{4}(a_2 - a_1) & b_2 &= -\tfrac{1}{3} - b_1 \\ x_1 &= 0 & x_2 &= 0 \end{aligned}$$

The parameters for I3 are

$$\begin{aligned} a_1 &= \frac{3}{2}\frac{1}{1+r} & a_2 &= ra_1 \\ b_1 &= 0 & b_2 &= 0 \\ x_1 &= \tfrac{1}{4} - \tfrac{1}{4}(a_2 - a_1) & x_2 &= \tfrac{1}{2} - x_1 \end{aligned}$$

The parameters for I5 are

$$\begin{aligned} a_1 &= \frac{14}{9}\frac{1}{1+r} & a_2 &= ra_1 \\ b_1 &= \tfrac{1}{18} - \tfrac{1}{8}(a_2 - a_1) & b_2 &= \tfrac{1}{9} - b_1 \\ x_1 &= \tfrac{1}{3} - \tfrac{3}{8}(a_2 - a_1) & x_2 &= \tfrac{2}{3} - x_1 \end{aligned}$$

REFERENCES

1. Lele SK. Compact finite difference schemes with spectral-like resolution. *Journal of Computational Physics* 1992; **103**:16–42.
2. Xiaolin Zhong. High-order finite-difference schemes for numerical simulation of hypersonic boundary layer transition. *Journal of Computational Physics* 1998; **144**:662–709.
3. Sesterhenn J. A characteristic-type formulation of the Navier–Stokes equations for high order upwind schemes. *Computers and Fluids* 2001; **30**:37–67.
4. Tolstykh AI, Lipavskii MV. On the performance of methods with third- and fifth-order compact upwind differencing. *Journal of Computational Physics* 1998; **140**:205–232.
5. Adams NA, Shariff K. A high-resolution hybrid compact-ENO scheme for shock–turbulence interaction problems. *Journal of Computational Physics* 1996; **127**:27–51.
6. Kennedy CA, Carpenter MH, Lewis RM. Low-storage, explicit Runge–Kutta schemes for compressible Navier–Stokes equations. *Applied Numerical Mathematics* 2000; **35**:177–219.
7. van Haaren MJ, Stoker HC, van den Boogaard AH, Huetink J. The ALE-method with triangular elements: direct convection of integration point values. *International Journal for Numerical Methods in Engineering* 2000; **49**:697–720.
8. Poinsot TJ, Lele SK. Boundary conditions for direct simulations of compressible viscous flows. *Journal of Computational Physics* 1992; **101**:104–129.
9. de Lange HC. Split time-integration for low-Mach number compressible flows. *Communications in Numerical Methods in Engineering* 2004; **20**(7):501–509.

